

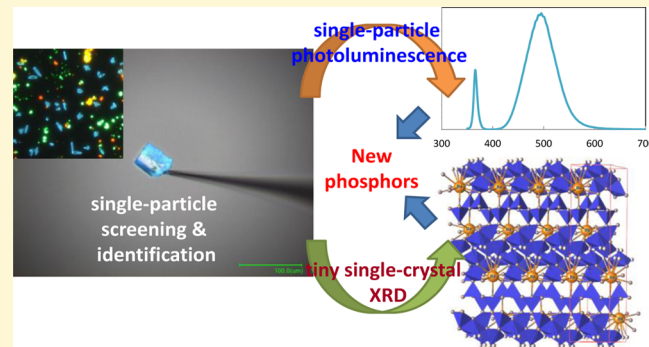
Discovery of New Nitridosilicate Phosphors for Solid State Lighting by the Single-Particle-Diagnosis Approach

Naoto Hirosaki, Takashi Takeda, Shiro Funahashi, and Rong-Jun Xie*

Sialon Group, Sialon Unit, Environment and Energy Materials Division, National Institute for Materials Science, Namiki 1-1, Tsukuba, Ibaraki 305-004, Japan

Supporting Information

ABSTRACT: Discovery of novel luminescent materials is of fundamental importance in the advancement of solid state lighting and flat panel display technologies. In this work, we report a single-particle-diagnosis method for the discovery of new phosphors by just characterizing a luminescent crystalline particle as small as $10\text{ }\mu\text{m}$ in diameter. We explored single-particle fluorescence imaging and spectroscopy techniques to evaluate the photoluminescence of a phosphor particle distinguished from a complex powder mixture and applied a high-resolution single-crystal X-ray diffractometer to determine its crystal structure. The approach enabled us to discover two new phosphors in the $\text{Ba}_3\text{N}_2-\text{Si}_3\text{N}_4-\text{AlN}$ ternary system: $\text{Ba}_5\text{Si}_{11}\text{Al}_7\text{N}_{25}:\text{Eu}^{2+}$ and $\text{BaSi}_4\text{Al}_3\text{N}_9:\text{Eu}^{2+}$. $\text{Ba}_5\text{Si}_{11}\text{Al}_7\text{N}_{25}:\text{Eu}^{2+}$ crystallizes in the space group of $Pnnm$ (no. 58) with $a = 9.5923(2)$, $b = 21.3991(5)$, $c = 5.8889(2)$ Å and $Z = 2$, while $\text{BaSi}_4\text{Al}_3\text{N}_9:\text{Eu}^{2+}$ in the space group of $P21/C$ (no. 14) with $a = 5.8465(4)$, $b = 26.7255(18)$, $c = 5.8386(4)$ Å, $\beta = 118.897^\circ$ and $Z = 4$. The single-particle photoluminescence of $\text{Ba}_5\text{Si}_{11}\text{Al}_7\text{N}_{25}:\text{Eu}^{2+}$ shows yellow emission ($\lambda_{\text{em}} = 568$ nm, fwhm = 98 nm) and a quantum efficiency of 36% under the 405 nm excitation. $\text{BaSi}_4\text{Al}_3\text{N}_9:\text{Eu}^{2+}$ shows blue emission ($\lambda_{\text{em}} = 500$ nm, fwhm = 67 nm) upon the 365 nm excitation.



I. INTRODUCTION

Lanthanide-doped luminescent materials have been utilized widely in applications from lighting and display to detecting and sensing.^{1–9} As a revolutionary lighting technology, solid state lighting promises to consume significantly less electricity and, thus, would address urgent challenges of greenhouse gas emissions, energy security, and economic revitalization.^{10–14} In this technology, luminescent materials play key roles by spectrally converting the ultraviolet or blue-light emitted from LED chips into useful blue-to-red emissions, thus determining the efficiency, color rendition, color temperature, reliability, and lifetime of the lighting devices.^{6,15–17} Rare earth-activated nitridosilicate phosphors, M–Si–(Al)–(O)–N:Re (M = alkaline earth or lanthanide metal, Re = rare earth activator), are emerging phosphors with great potentials to substantially enhance the luminous efficiency, color rendition, and lifetime of white light-emitting diodes (LEDs), which usually offers significantly red-shifted photoluminescence, abundant emission colors, high quantum efficiency, and very small thermal quenching.^{6,16–18} The excellent photoluminescence properties rely largely on the covalent and short Re–N chemical bonds and on the highly condensed structure built up on the corner-sharing or edge-sharing SiN₄ tetrahedral framework. Moreover, several nitridosilicate phosphors, such as α -sialon:Eu²⁺,¹⁹ β -sialon:Eu²⁺,²⁰ CaAlSiN₃:Eu²⁺,²¹ Sr₂Si₅N₈:Eu²⁺,²² and La₃Si₆N₁₁:Ce³⁺,²³ have been commercialized shortly after they

are discovered, thereby vindicating the superiority of nitridosilicate phosphors over others. In addition to their applications in lighting, nitridosilicate luminescent materials can also be utilized in field emission displays (emissive materials) and solar cells (down-conversion materials) as well.^{24,25}

Increasingly demanded by newly developed solid state lighting technologies and devices, new nitridosilicate phosphors with enhanced or specialized properties are continuously pursued by chemists or materials scientists. There are two classical methods of searching for new luminescent materials. The first one is to comprehensively interrogate all possible nitridosilicate compounds in the Inorganic Crystal Structure Database (ICSD), which occasionally leads to the discovery of notable α -sialon:Eu²⁺,¹⁹ β -sialon:Eu²⁺,²⁰ CaAlSiN₃:Eu²⁺,²¹ and AlN:Eu²⁺²⁴ phosphors. The second one is to grow and determine the crystal structure of a large-sized single crystal, which for example identifies Ba₂Si₅N₈:Eu²⁺, SrAlSi₄N₇:Eu²⁺, Sr₂Al_{5+x}Si_{2.1-x}N_{3.5-x}O_{2+x}:Eu²⁺, Ba₃Ga₃N₅:Eu²⁺, and Ba₂AlSi₃N₉:Eu²⁺.^{26–30} Both methods, however, are definitely slow and labor intensive. The former requires an iterative procedure of powder processing to achieve a phase pure powder, and the latter faces challenges of growing a single

Received: May 22, 2014

Revised: June 17, 2014

Published: June 17, 2014



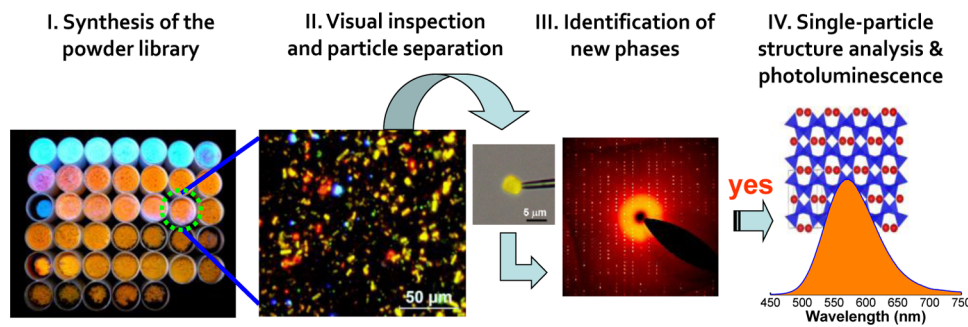


Figure 1. Schematics of the single-particle-diagnosis approach.

crystal with large size (typically larger than 100 μm in all dimensions), high purity, and high quality (i.e., free of cracks or twinning). Therefore, it is desirable to find a way that allows the high-speed discovery of new phosphors, removing the need to prepare a perfect single crystal or a phase-pure powder.

The combinatorial chemistry approach has been successfully utilized to high-throughput screening and optimizing luminescent materials.^{31–34} However, the luminescent materials discovered so far cannot be considered as real “novel” phosphors but new or optimized compositions, as the crystal structure of end members are already known. Furthermore, the photoluminescence must be exclusively mapped on a single phase. Otherwise, photoluminescence properties (e.g., chromaticity coordinates and luminescence intensity) cannot be precisely characterized. The pioneer work on combinatorial synthesis of nitridosilicate luminescent materials is done by Sohn, where a heuristic optimization approach consisting of a nondominated-sorting genetic algorithm (NSGA) and particle swarm optimization (PSO) is used simultaneously.^{35–38} Several nitridosilicate phosphors with new crystal structures have been discovered, including $\text{Ca}_{15}\text{Si}_{20}\text{N}_{30}\text{O}_{10}:\text{Eu}^{2+}$, $\text{Ba}_{1.5}\text{Ca}_{0.5}\text{Si}_5\text{N}_6\text{O}_3:\text{Eu}^{2+}$, and $\text{La}_{4-x}\text{Ca}_x\text{Si}_{24}\text{O}_{3+x}\text{N}_{18-x}:\text{Eu}^{2+}$.^{35–37} This improved combinatorial synthesis method greatly speeds up the discovery of new phosphors, but it still has several weak points. First, the heuristics optimization is a two-step process (i.e., NSGA and PSO), and in each step, it requires the resynthesis of powders for at least five times before the fitness functions are converged to an optimal value. Second, the structural determination from the powder X-ray diffraction patterns is very time-consuming and uncertain due to the random orientation of individual microcrystals. Lastly, the powder sample must have a very high degree of phase purity to attain the precise structural analysis.

The weakness of traditional and modified combinatorial methods mentioned above can be overcome if suitable microscale characterization techniques are available. These techniques are required to explore the crystal structure and photoluminescence at a single-particle level. In this work, we proposed to use single-crystal X-ray diffraction together with single-particle fluorescence imaging and spectroscopy as microscale tools for rapidly accomplishing phase identification, photoluminescence properties assessment, and structural determination of a single microcrystalline phosphor particle with a diameter down to 10 μm . The single luminescent crystalline particle of new phosphors, which is equivalent to a small single crystal grown in a complex powder mixture, was then visualized, pinpointed, and precisely characterized finally (both structure and photoluminescence). Using this approach, we examined the $\text{Ba}_3\text{N}_2-\text{Si}_3\text{N}_4-\text{AlN}$ ternary system and

discovered two interesting nitridosilicate phosphors that are potentially used in solid state lighting. The crystal structure and the single-particle photoluminescence of the newly discovered phosphors were reported in this investigation.

II. CONCEPT OF THE APPROACH

Inspired by mapping out phase diagrams using microscale probes for a variety of properties such as thermal conductivity, dielectric properties, thermoelectric properties, magnetic properties, and optical properties,^{39,40} we report a single-particle-diagnosis approach for rapidly characterizing a small microcrystalline phosphor particle distinguished from a powder mixture containing different crystalline phases. The principle of the approach is straightforward: to treat an individual luminescent particle in a complex mixture as a tiny single crystal, distinguish it by its characteristic emission color, morphology and size, and finally to determine its structure and property using microscale characterization techniques such as super-resolution single-crystal X-ray diffraction, single-particle fluorescence imaging and spectroscopy. As illustrated in Figure 1, there are four steps in this approach. Step I, phosphor powder samples with varying compositions (sample library) are synthesized via a traditional solid state reaction. Step II, the phosphor powders are visually inspected and imagined using a digital optical microscope coupled with an ultraviolet lighting source. The luminescent particles are straightforwardly distinguished on the basis of their emission color and morphology. Step III, luminescent particles with new crystal structure are screened and identified by preliminarily measuring their lattice parameters using a single-crystal X-ray diffractometer. The particle with lattice parameters matching well with those stored in the structure database (ICSD) will be ruled out. Step IV, the structure of the new phase is then explored in a more detail and the photoluminescence properties are measured using single-particle fluorescence spectroscopy.

Appropriate and accurate microprobe tools that enable to identify a single particle are the key to apply this method. First, we use Eu^{2+} or Ce^{3+} as a labeling tool because its luminescence is structurally dependent and can also be visualized (luminescence mapping). Only luminescent particles are screened and identified in this approach. Second, we apply a fine-focus single-crystal X-ray diffractometer with superhigh resolution to carry out both the preliminary and final structure analysis of a single luminescent particle. The high resolution, achieved by using a charge-coupled devices (CCD) area detector and multilayer focusing mirrors, enables to determine the crystal structure of a tiny microcrystal that has a size 2 orders of magnitude smaller than single crystals routinely used for structural analysis. Third, we build a single-particle

fluorescence spectroscopy system to perform photoluminescence property measurements (spectra, thermal quenching and quantum efficiency) of a luminescent particle (Figure 2). The

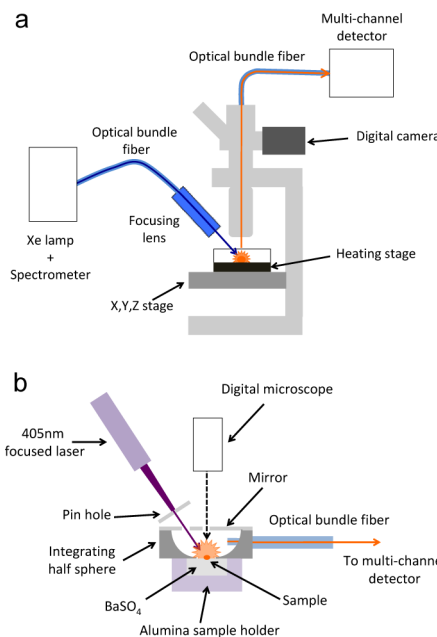


Figure 2. Schematics of home-built single-particle fluorescence microspectroscopy setups for measuring (a) photoluminescence spectra, and (b) quantum efficiency.

accuracy of the system is acceptable for a fine particle, which is confirmed by using Ca- α -sialon:Eu²⁺ as a reference (Supporting Information Figure S1). The excitation spectrum of a Ca- α -sialon:Eu²⁺ particle was blue-shifted by \sim 30 nm at the right wing in comparison with that of the powder, which is caused by the absence of reabsorption of luminescence for a particle. Due to the absence of reabsorption, the particle exhibited an emission band slightly blue-shifted by \sim 3 nm at the left wing compared with the powder sample. The temperature-dependent luminescence of a Ca- α -sialon:Eu²⁺ particle duplicated that of the powder at temperatures below 150 °C. The divergence (\sim 6%) at temperatures higher than 150 °C was due to the difference between sample temperature and set temperature. The quantum efficiency of the particle was measured as 80% (excited at 405 nm) comparable to that of the powder sample.

III. EXPERIMENTAL SECTION

Sample Preparation. Twenty samples in the Ba₃N₂–Si₃N₄–AlN ternary system, with varying Ba:Si:Al ratios, were prepared by firing appropriate amounts of Ba₃N₂ (Cerac, 99.7%, \sim 20 mesh), Si₃N₄ (Ube, E-10), AlN (Tokuyama, E grade) and EuN (homemade) at 1900 °C for 2 h in 1.0 MPa N₂ atmosphere using a gas-pressure sintering furnace (FVPHR-R-10, FRET-40). The Eu concentration was fixed at 5 mol % with respect to Ba.

Sample Selection and Assembly. The powder samples were visualized in a digital optical microscope (BX51M) under the ultraviolet excitation (a 365 nm UV-LED). The luminescent particle was then separated individually depending on their emission colors and particle size and mounted on the tip of a fine glass fiber using an epoxy. The fiber was attached to a brass mounting pin, and the pin was then inserted into the goniometer head.⁴⁴

Structural Analysis. Single-crystal XRD data of a single particle were collected on a SMART APEX II Ultra diffractometer with Mo K α radiation ($\lambda = 0.71073 \text{ \AA}$) and multilayer mirrors as monochromator, operated at 50 kV and 50 mA. Applied absorption corrections were done using the multiscan procedure SADABS.⁴¹ The structure was solved by direct methods implemented in SHELSX-97.⁴² Refinement of crystal structures was carried out with anisotropic displacement parameters for all atoms by full-matrix least-squares calculation on F2 in SHEXL-97.⁴³

Chemical Composition. The elemental analysis was carried out on carbon-coated particles using a scanning electron microscopy (SU1510) equipped with an energy dispersive spectroscopy (XFlash SDD) operated at 15 kV.

Photoluminescence and Thermal Quenching. The phosphor particle mounted on a cover glass was excited by a monochromatized 150W Xe lamp (QE1100, Otsuka electronics) through optical bundle fiber and focusing lens. The emission and excitation spectra were recorded by a multi-channel photo detector (MCPD7700, Otsuka electronics) through an optical bundle fiber attached to an optical microscope (BX51M, objective lens 10 \times -50 \times , Olympus) (Figure 2a). Due to the absorption of lens glass and the sensitivity of the detector, the excitation spectrum was measured in the range of 350–600 nm. The temperature-dependent luminescence (25–300 °C) of a phosphor particle was evaluated with a computer-controlled stage heater (THMS600, Linkam Scientific Instruments) installed in the system (Figure 2a). Considering the movement of the particle due to thermal expansion of heater parts and glass plate, the position of the particle (x, y, z) was adjusted to the initial state from time to time with the aid of microscopic image stored at room temperature. The actual temperature of the single particle upon heating might be somewhat higher than the temperature reading on the display, because the particle could be also heated by the Xe lamp irradiation. The heat generated by the irradiation was not calibrated because it was hardly measured on such a small particle.

Quantum Efficiency. For the quantum efficiency measurement (Figure 2b), a single particle phosphor mounted on the BaSO₄ (Wako Pure Chemical Industries) was positioned at the bottom of a 1 in. semi-integrating sphere having two holes for the sample and photo detector installation (HalfMoon, Otsuka electronics). The mirror part at the equatorial plane has also two holes for the excitation light and microscope observation (blocked during measurement). A 405 nm semiconductor laser (SU-61-405, Audio-technica) light was irradiated on the center of the particle phosphor with the aid of microscope image. A handmade pinhole (260 μm) was placed near the semi-integrating sphere to reduce the beam size of the laser light down to \sim 50 μm in diameter. The luminescence spectrum of the phosphor particle and the reflected light of both the particle and BaSO₄ were measured in the range of 330–800 nm by a multichannel photo detector (MCPD7700, Otsuka electronics). The calibration parameter to the energy scale was obtained by dividing the parameter from a Lambertian diffuser (Spectralon, Labsphere) by the one from the measurement system (microscopy, semi-integrating sphere). The internal quantum efficiency of the particle was calculated by the following equation⁴⁴

$$\eta_i = \frac{\int \lambda \bullet P(\lambda) d\lambda}{\int \lambda \{E(\lambda) - R(\lambda)\} d\lambda}$$

where $E(\lambda)/h\nu$, $R(\lambda)/h\nu$ and $P(\lambda)/h\nu$ are the number of photons in the spectrum of excitation, reflectance, and emission of the phosphor, respectively.

IV. RESULTS AND DISCUSSION

Visualization of Samples. The luminescence images of the irradiated powders with compositions no. 1–3 are shown in Figures 3b–c. In some cases, the unreacted starting powder of Si_3N_4 or AlN was also present but had no luminescence, so that it was submerged in the background. Obviously, the intuitive emission color of a composition is actually the accumulation of

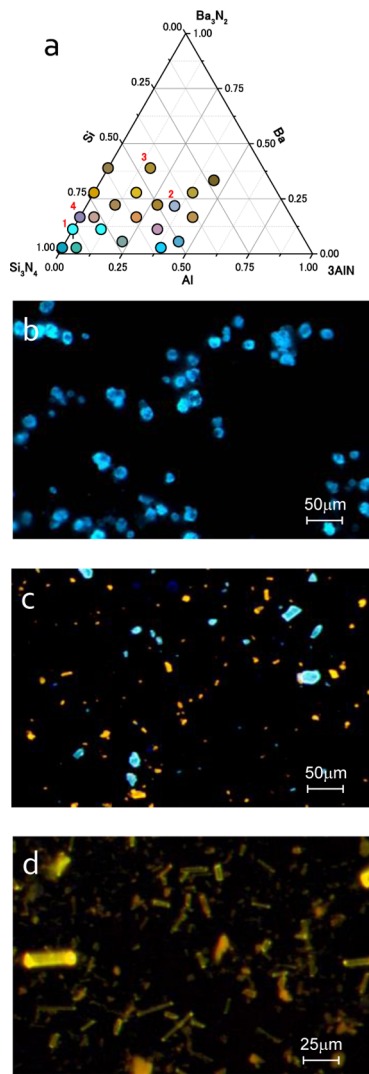


Figure 3. Powder library and luminescent particle(s). (a) Phase diagram of the ternary Ba_3N_2 - Si_3N_4 - AlN system showing the compositions investigated and their intuitive emission colors. (b) Microscopic image of diamond-like blue-emitting phosphor particles (composition no. 1, $\text{Ba}:\text{Si}:\text{Al} = 0.11:0.89:0$) in a single phase powder. (c) Microscopic image of mixed luminescent particles with two different emission colors (composition no. 2, $\text{Ba}:\text{Si}:\text{Al} = 0.22:0.11:0.67$). (d) Microscopic image of mixed luminescent particles with three different emission colors and morphologies (composition no. 3, $\text{Ba}:\text{Si}:\text{Al} = 0.39:0.44:0.17$).

colors from individual luminescent particles, and the particle with a different color principally implies a different crystalline phase. The particles are seen to have a size of about several to several ten micrometers, which are much smaller than single crystals normally grown for structural determination. Moreover, due to different growth habits the particles exhibited varying morphologies. Six luminescent particles with different colors and morphologies were clearly seen, with a blue one in Figure 3b, blue and orange ones in Figure 3c, and yellow (need-like), orange (plate-like) and red (rod-like or rice grain-like) ones in Figure 3d.

Identification of New Luminescent Materials. Luminescent particles with distinct colors and shapes were distinguished from the multicolored powder mixture and then individually amounted to a glass fiber for X-ray diffraction, as shown in Figure 4. We first identified whether the selected phosphor particle had a new crystal structure or not. This was done by collecting diffraction patterns of the particle in all directions using a single crystal X-ray diffractometer, followed by preliminarily calculating lattice parameters. The particle with lattice parameters not matching with those stored in ICSID was recognized as a new crystalline phase, and it thus entered into next round of characterization. The diamond-like blue (Figure 4a), plate- and diamond-like orange (Figure 4c, e), rice grain-like red (Figure 4d), and triangle blue (Figure 4g) particles were identified as already known Eu^{2+} -doped $\text{BaSi}_5\text{N}_{10}$,⁴⁵ $\text{Ba}_2\text{Si}_5\text{N}_8$ (diamond and plate-like),²⁶ $\text{Ba}_2\text{Si}_5\text{AlN}_9$,³⁰ and BaSi_6N_8 ,⁴⁶ respectively. On the other hand, the diamond-like cyan (Figure 4b) and needle-like yellow particles (Figure 4f) were labeled as new phosphors with uncovered crystal structures. It is obviously seen that several different crystalline phases can be identified rapidly at the same time by just diagnosing a single particle. Sixteen other compositions were identified to be either the mixture of known phases or the mixture of known phases and the unknown phase mentioned above.

Structural Determination. The yellow particle, $\text{Ba}_5\text{Si}_{11}\text{Al}_7\text{N}_{25}$, was finally refined in the orthorhombic space group $Pnnm$ (no. 58) with $a = 9.5923(2)$ Å, $b = 21.3991(5)$ Å, $c = 5.8889(2)$ Å, $\alpha = \beta = \gamma = 90^\circ$, and $Z = 2$ (Tables 1 and 2 and Supporting Information Tables S1 and S2). The chemical composition was measured as $\text{Ba}:\text{Eu}:\text{Si}:\text{Al} = 8.73:0.52:21.73:13.60$, which is in accordance to $\text{Ba}:\text{Eu}:\text{Si}:\text{Al} = 8.73:0.46:20.22:12.87$ based on the structural model. This new nitridosilicate compound contains a highly condensed framework built-up on SiN_4 and AlN_4 tetrahedra (Figure 5). In $\text{Ba}_5\text{Si}_{11}\text{Al}_7\text{N}_{25}$, the tetrahedra are mostly linked via common corners, but the structure also contains edge-shared tetrahedra for Si_7 . Both Si and Al atoms share the equivalent site with disorder distribution, which are also found in CaAlSiN_3 .²¹ The framework of $\text{Ba}_5\text{Si}_{11}\text{Al}_7\text{N}_{25}$ host three different Ba positions that are coordinated to 11 (Ba1), 10 (Ba2), and 8 (Ba3) nitrogen atoms, respectively (Figure 5). The Ba(Eu)-N bond lengths vary between 2.838(2) and 3.030(3) Å for Ba1, between 3.003(2) and 3.354(2) Å for Ba2, and between 2.719(3) and 3.083(2) Å for Ba3. These distances are slightly longer than already known barium nitridosilicates (e.g., $\text{Ba}_2\text{AlSi}_5\text{N}_9$, 2.55–3.68 Å, $\text{Ba}_2\text{Si}_5\text{N}_8$, 2.68–3.00 Å⁴⁷).

The crystal structure of the new blue-emitting particle, $\text{BaSi}_4\text{Al}_3\text{N}_9:\text{Eu}^{2+}$, was also determined by using the single crystal X-ray diffraction. It crystallized in monoclinic system and the space group is $P21/C$ (no. 14) with $a = 5.8465(4)$ Å, $b = 26.7255(18)$ Å, $c = 5.8386(4)$ Å, $\beta = 118.897^\circ$, and $Z = 4$.

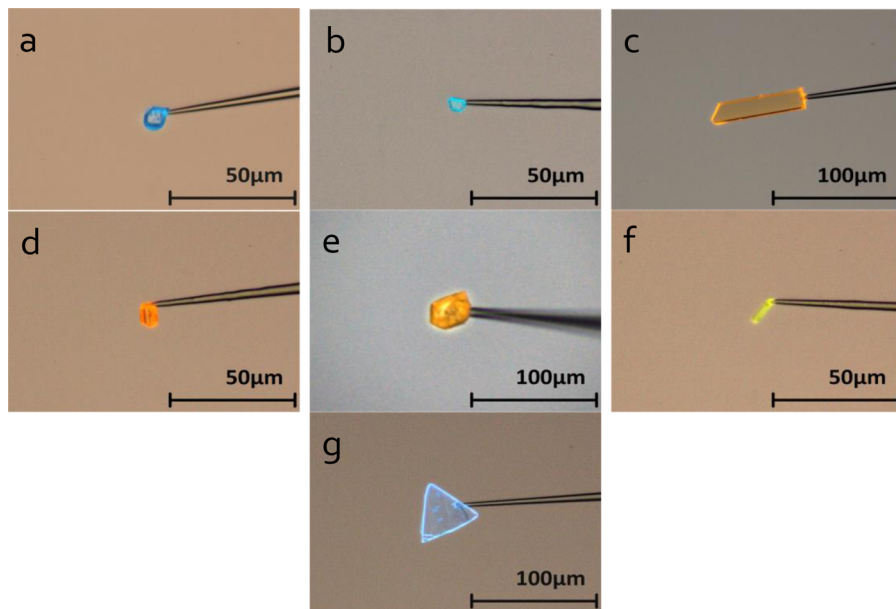


Figure 4. Luminescent particles with different emission colors and morphologies for structural analysis. (a) Diamond-like blue particle with a size of $7 \times 7 \times 9 \mu\text{m}$ from composition no. 1. (b) Diamond-like cyan particle with a size of $4 \times 5 \times 6 \mu\text{m}$ from composition no. 2. (c) Plate-like red particle with a size of $5 \times 18 \times 80 \mu\text{m}$ from composition no. 2. (d) Rice grain-like red particle with a size of $2 \times 6 \times 8 \mu\text{m}$ from composition no. 3. (e) Diamond-like orange particle with a size of $26 \times 32 \times 35 \mu\text{m}$ from composition no. 3. (f) Needle-like yellow particle with a size of $3 \times 3 \times 10 \mu\text{m}$ from composition no. 3. (g) Triangle cyan particle with a size of $3 \times 49 \times 50 \mu\text{m}$ from composition no. 4 ($\text{Ba:Si:Al} = 0.167:0.833:0$).

Table 1. Crystal Data and Refinement Details of $\text{Ba}_5\text{Si}_{11}\text{Al}_7\text{N}_{25}$ and $\text{BaSi}_4\text{Al}_3\text{N}_9$

	$\text{Ba}_5\text{Si}_{11}\text{Al}_7\text{N}_{25}$	$\text{BaSi}_4\text{Al}_3\text{N}_9$
formula mass/g·mol ⁻¹	1538.41	457.43
crystal system	Orthorhombic	Monoclinic
space group	<i>Pnnm</i>	<i>P21/c</i>
cell parameters/Å	<i>a</i> = 9.5928(2) <i>b</i> = 21.3991(5) <i>c</i> = 5.8889(2)	<i>a</i> = 5.8465 (4) <i>b</i> = 26.7255 (18) <i>c</i> = 5.8386 (4)
β /°	90	118.897(10)
<i>V</i> /Å ³	1208.85(9)	798.70(9)
density/g·cm ⁻³	4.226	3.818
<i>Z</i>	2	4
crystal size/mm ³	0.06 × 0.01 × 0.01	0.10 × 0.08 × 0.02
diffractometer	Bruker APEXII CCD area detector	
radiation type	Mo K α ($\lambda = 0.71073 \text{\AA}$)	
abs correction	Multiscan (SADABS)	
measured reflns	27481	12205
independent reflections	2889	3719
observed reflns	2420	2824
<i>R</i> [$F^2 > 2\sigma(F^2)$]	0.024	0.020
w <i>R</i> (F^2)	0.054	0.062
<i>S</i>	1.05	1.50

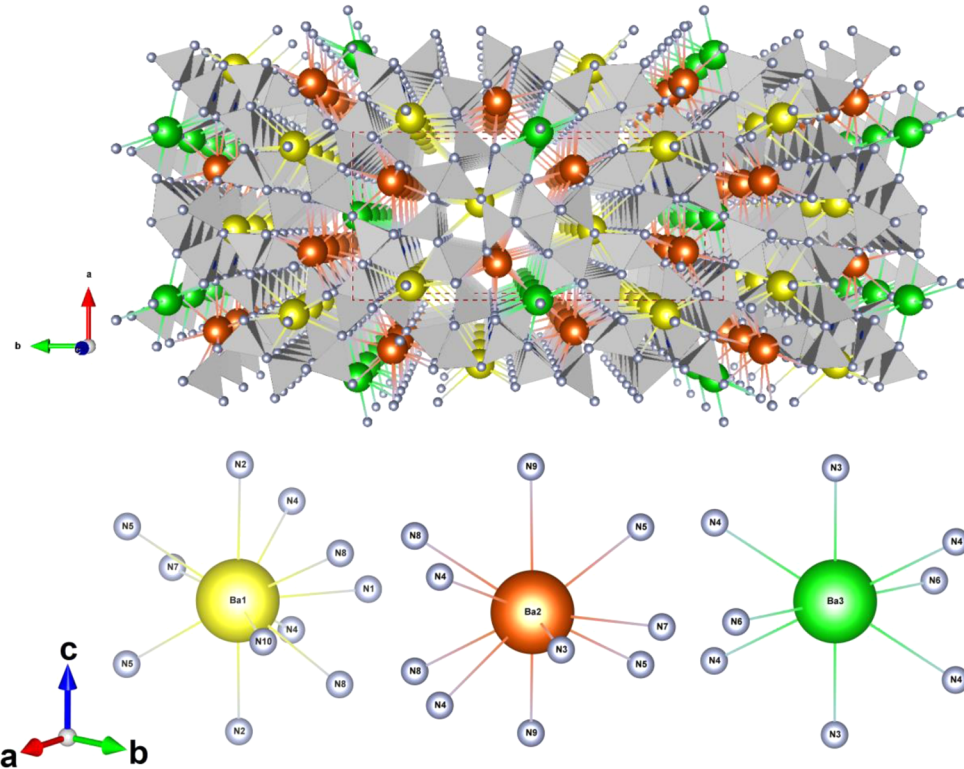
(Supporting Information Tables S3 and S4). There is only one crystallographic site for Ba that is coordinated to 11 nitrogen atoms. The distances of Ba(Eu)–N are between 2.970 (19) and 3.497 (3) Å, with an average length of 3.164 Å. These are longer than most barium nitridosilicates mentioned above, but comparable to the distances of Ba–N in $\text{BaSi}_7\text{N}_{10}$ (2.91–3.53 Å).⁴⁸

Single-Particle Photoluminescence Properties. Photoluminescence of a single $\text{Ba}_5\text{Si}_{11}\text{Al}_7\text{N}_{25}:\text{Eu}^{2+}$ particle are given in Figure 6. It showed a broad emission band centered at ~570 nm and a full width at half-maximum (fwhm) of 98 nm. The excitation spectrum displayed a band with a tail extending to

550 nm (Figure 6b), matching well with the emission of blue LEDs. For the powder sample, the excitation spectrum at the right wing will be expected to be greatly enhanced as a result of reabsorption, leading to a much broader band. This yellow phosphor has the emission wavelength of ~15 nm shorter than Ca- α -sialon:Eu²⁺.^{6,17,19} The luminescence of the new yellow phosphor declined by 35% at 150 °C. The thermal quenching temperature (at which the luminescence reduces by 50%) was ~190 °C (Figure 6c), which is comparable to YAG:Ce³⁺.⁴⁹ The internal quantum efficiency of the particle was calculated as 36.4% (Supporting Information Figure S2). To vindicate the reliability of the system, the measurement was also carried out

Table 2. Atomic Coordinates, Occupancies, and Isotropic Atomic Displacement Parameters of $\text{Ba}_{4.75}\text{Eu}_{0.25}\text{Si}_{11}\text{Al}_7\text{N}_{25}$

	<i>x</i>	<i>y</i>	<i>z</i>	$U_{\text{iso}}^*/U_{\text{eq}}$	occupied
Ba1	0.41564 (2)	0.34264 (2)	0.5	0.01121 (5)	0.95
Ba2	0.79034 (3)	0.39208 (2)	0.5	0.01828 (6)	0.95
Ba3	1	0.5	0	0.03805 (14)	0.95
Eu1	0.41564 (2)	0.34264 (2)	0.5	0.01121 (5)	0.05
Eu2	0.79034 (3)	0.39208 (2)	0.5	0.01828 (6)	0.05
Eu3	1	0.5	0	0.03805 (14)	0.05
Si1	0.55083 (10)	0.39370 (4)	0	0.00403 (15)	0.6111
Si2	0.22020 (11)	0.38886 (5)	0	0.00840 (17)	0.6111
Si3	0.11764 (10)	0.43589 (5)	0.5	0.00557 (16)	0.6111
Si4	0.28278 (10)	0.20807 (4)	0.5	0.00452 (16)	0.6111
Si5	0.07340 (7)	0.30125 (3)	0.25365 (11)	0.00525 (12)	0.6111
Si6	0.34398 (11)	0.26504 (5)	0	0.00665 (17)	0.6111
Si7	0.37537 (7)	0.48606 (3)	0.24506 (12)	0.00658 (12)	0.6111
Al1	0.55083 (10)	0.39370 (4)	0	0.00403 (15)	0.3889
Al2	0.22020 (11)	0.38886 (5)	0	0.00840 (17)	0.3889
Al3	0.11764 (10)	0.43589 (5)	0.5	0.00557 (16)	0.3889
Al4	0.28278 (10)	0.20807 (4)	0.5	0.00452 (16)	0.3889
Al5	0.07340 (7)	0.30125 (3)	0.25365 (11)	0.00525 (12)	0.3889
Al6	0.34398 (11)	0.26504 (5)	0	0.00665 (17)	0.3889
Al7	0.37537 (7)	0.48606 (3)	0.24506 (12)	0.00658 (12)	0.3889
N1	0.1554 (3)	0.26920 (14)	0.5	0.0091 (5)	1
N2	0.3968 (3)	0.34725 (14)	0	0.0089 (5)	1
N3	0	0.5	0.5	0.0148 (9)	1
N4	0.1065 (2)	0.38423 (11)	0.2587 (4)	0.0125 (4)	1
N5	0.5364 (2)	0.44072 (10)	0.7580 (4)	0.0087 (3)	1
N6	0.2767 (3)	0.47234 (14)	0	0.0090 (5)	1
N7	0.2864 (3)	0.47186 (15)	0.5	0.0105 (5)	1
N8	0.3929 (2)	0.22054 (10)	0.2543 (4)	0.0097 (4)	1
N9	0.7115 (4)	0.36319 (17)	0	0.0190 (7)	1
N10	0.1539 (3)	0.27463 (17)	0	0.0130 (6)	1

**Figure 5.** Crystal structure of newly discovered $\text{Ba}_5\text{Si}_{11}\text{Al}_7\text{N}_{25}:\text{Eu}^{2+}$. Structure viewed along the [001] direction (upper) and three coordination numbers of Ba (Eu) (below).

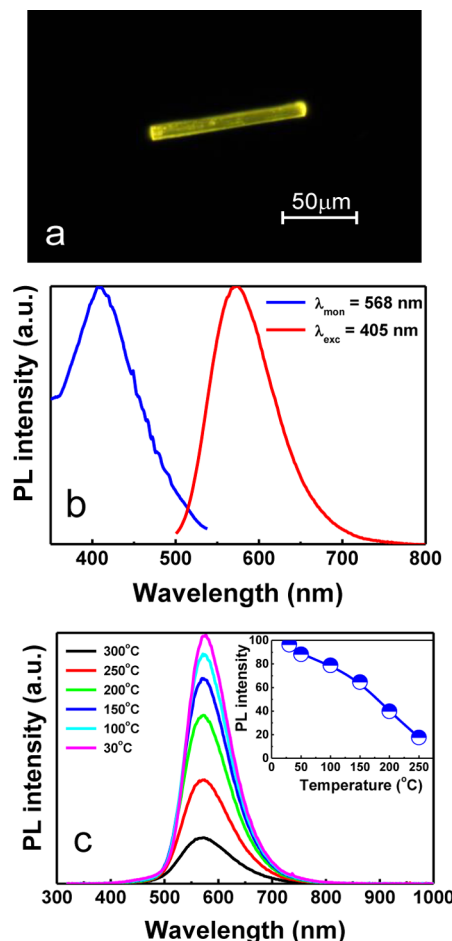


Figure 6. Photoluminescence properties measured on a single phosphor particle of $\text{Ba}_5\text{Si}_{11}\text{Al}_7\text{N}_{25}:\text{Eu}^{2+}$. (a) Needle-like particle used for measurements, the particle size was $5 \times 6 \times 75 \mu\text{m}$. (b) Emission and excitation spectra. (c) Thermal quenching.

on a mixture of seven particles. The quantum efficiency of the particle aggregate, averaged on eight times of run, was $36.7 \pm 4.2\%$, which is in a good agreement with that of a single one. These results indicate that this yellow phosphor exhibits promising photoluminescence properties, and can be potentially used to create white light when coupled with a blue LED.

The emission spectrum of $\text{BaSi}_4\text{Al}_3\text{N}_9:\text{Eu}^{2+}$, also measured on one single particle upon the 365 nm excitation, shows a relatively narrow band with a peak maximum at 500 nm and a fwhm of 67 nm (Figure 7). The blue-shifted emission spectrum

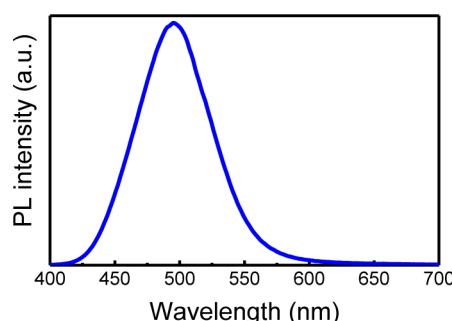


Figure 7. Emission spectrum of a single particle of $\text{BaSi}_4\text{Al}_3\text{N}_9:\text{Eu}^{2+}$. The spectrum was measured under the 365 nm excitation.

of $\text{BaSi}_4\text{Al}_3\text{N}_9:\text{Eu}^{2+}$ (versus $\text{Ba}_5\text{Si}_{11}\text{Al}_7\text{N}_{25}:\text{Eu}^{2+}$) can be ascribed to the large coordination number of Ba (Eu) and long distances of Ba(Eu)-N that lead to small crystal field splitting and nephelauxetic effect.

V. CONCLUSIONS

In this study, we demonstrate that the single-particle-diagnosis approach provides a simple and high-speed way to discover new luminescent materials, by only characterizing a luminescent particle distinguished from a complex powder mixture that is arbitrarily prepared. This revolutionary method not only significantly saves times of not growing a large-size single crystal or purifying a powder mixture but also has the same high precision as the classical method using a single crystal for structural determination. The use of a super-resolution single crystal X-ray diffractometer enables analysis of the crystal structure of a tiny single crystal, which substantially enhance the flexibility of selecting target microcrystalline particles in various material systems. Compared with traditional methods, our approach is capable of evaluating photoluminescence properties (i.e., spectra, thermal quenching, and quantum efficiency) of a single phosphor particle by using single-particle fluorescence spectroscopy, which therefore needs not synthesize phase-pure powders for property assessments. Moreover, the single particle photoluminescence properties can serve as selection criteria for a phosphor discovered, which determines whether the scale-up synthesis of powders is further needed or not. This again remarkably saves time, energy, and labor intensity by not preparing “bad” phosphor powders with great efforts.

In classical combinatorial methods, the search for new phosphors in the ternary system is required to screen the compositions as much as possible, and the ratio intervals of end members must be set to be as small as possible to reach a high degree of phase purity. This will lead to a large number of compositions to be synthesized, and the number is further increased if the processing conditions (i.e., holding time and temperature) are altered. In our approach, a phase-pure powder mixture is not a requirement, only several tens of compositions are, thus, enough to identify new luminescent materials. This is due to the fact that in an arbitrarily synthesized composition it definitely contains phase(s) that also appear in neighboring compositions if it fails to obtain a single phase. The luminescent particles with new crystal structures can then be distinguished and identified using the microscale characterization techniques.

It cannot be taken for granted that phase-pure powder samples of the discovered phosphor can be naturally prepared starting from the chemical composition of the single crystal. The actual chemical composition of a powder sample is sometimes deviated from that of a single crystal. A typical sample for this case is $\text{SrAlSi}_4\text{N}_7:\text{Eu}^{2+}$, where a single phase of the powder phosphor is finally achieved by intentionally adding double amount of AlN.⁵⁰ This difference is ascribed to the very strict local environment (e.g., chemical composition, compositional homogeneity, volume and composition of the transient liquid phase, temperature, etc.) required for a single crystal. To prepare phosphor powders with high phase purity, it is therefore suggested that some key factors, such as raw nitride materials (typically the oxygen content), nominal composition, flux materials, firing temperature, and gas pressure, should be carefully chosen and controlled.

The newly discovered $\text{Ba}_5\text{Si}_{11}\text{Al}_7\text{N}_{25}:\text{Eu}^{2+}$ yellow phosphor shows interesting photoluminescence for white LED applications, although its thermal stability and quantum efficiency are

somewhat underestimated when measuring on a single particle. The underestimation is due to the lack of reabsorption in a single particle and the larger size of the laser beam irradiating on a smaller particle, both of which enhances the light reflection. But anyhow, it is required to significantly enhance the quantum efficiency and thermal properties of $\text{Ba}_5\text{Si}_{11}\text{Al}_7\text{N}_{25}:\text{Eu}^{2+}$. The combinatorial composition spread technique would be one of the best choices to optimize the composition and photoluminescence properties of $\text{Ba}_5\text{Si}_{11}\text{Al}_7\text{N}_{25}:\text{Eu}^{2+}$ by the cationic (e.g., $\text{Sr} \rightarrow \text{Ba}$) or ionic (e.g., $\text{O} \rightarrow \text{N}$) substitution strategies.⁵¹ It implies that the combination of our approach (to discover new luminescent materials) with the combinatorial chemistry method (to optimize the composition of new luminescent materials) allows the high-speed identification of luminescent materials with promising properties.

Unambiguously, our approach can also be applicable to other luminescent material systems such as oxides, fluorides, sulfides, etc. Prospectively, it seems feasible to apply our concept to other solid state materials such as catalytic, magnetic, dielectric, and thermoelectric materials, given that corresponding microscale characterization techniques are available.^{40,41,52,53}

■ ASSOCIATED CONTENT

Supporting Information

Atomic displacement parameters, bond lengths, atomic coordinates, occupancies, photoluminescence properties, quantum efficiency measurement, and CIF files. This material is available free of charge via the Internet at <http://pubs.acs.org>.

■ AUTHOR INFORMATION

Corresponding Author

*E-mail: Xie.Rong-Jun@nims.go.jp.

Notes

The authors declare no competing financial interest.

■ ACKNOWLEDGMENTS

We thank K. Nakajima for help with experiments. We also thank T. Seuhiro, Y. Michiue, and K. Takahshi for discussions. The financial support of the JSPS KAKENHI (no. 23560811) is acknowledged.

■ REFERENCES

- (1) Wegh, R. T.; Donker, H.; Oskam, K. D.; Meijerink, A. *Science* **1999**, *283*, 663–666.
- (2) Bunzli, J. C. G.; Piguet, C. *Chem. Soc. Rev.* **2005**, *34*, 1049–1077.
- (3) Wang, F.; Han, Y.; Lim, C. S.; Lu, Y.; Wang, J.; Xu, J.; Chen, H.; Zhang, C.; Hong, M.; Liu, X. G. *Nature* **2010**, *463*, 1061–1065.
- (4) Pan, Z.; Lu, Y. Y.; Liu, F. *Nat. Mater.* **2012**, *11*, 58–63.
- (5) Wang, L.; Li, Y. D. *Chem. Mater.* **2007**, *19*, 727–734.
- (6) Xie, R.-J.; Li, Y. Q.; Hirosaki, N.; Yamamoto, H. *Nitride Phosphors and Solid State Lighting*; CRC Press: Boca Raton, FL, 2011.
- (7) Schmiechen, S.; Schneider, H.; Wagatha, P.; Hecht, C.; Schmidt, P. J.; Schnick, W. *Chem. Mater.* **2014**, *26*, 2712–2719.
- (8) Shirasaki, Y.; Supran, G. J.; Bawendi, M. G.; Bulovic, V. *Nat. Photonics* **2013**, *7*, 13–23 (2013).
- (9) Huang, X. Y.; Han, S. Y.; Huang, W.; Liu, X. G. *Chem. Soc. Rev.* **2013**, *42*, 172–201.
- (10) Ponce, F. A.; Bour, D. P. *Nature* **1997**, *386*, 351–359.
- (11) Zukauskas, A.; Shur, M. S.; Gaska, R. *Introduction to solid state lighting*; John Wiley & Sons. Inc.: New York, 2002.
- (12) Steigerwald, D. A.; Bhat, J. C.; Collins, D.; Fletcher, R. M.; Holcomb, M. O.; Ludowide, M. J.; Martin, P. S.; Rudaz, S. L. *IEEE J. Sel. Top. Quantum Electron.* **2002**, *8*, 310–320.
- (13) Schubert, E. F.; Kim, J. K. *Science* **2005**, *308*, 1274–1278.
- (14) Schubert, E. F.; Kim, J. K.; Luo, H.; Xi, J. Q. *Rep. Prog. Phys.* **2006**, *69*, 3069–3099.
- (15) Ye, S.; Xiao, F.; Pan, Y. X.; Ma, Y. Y.; Zhang, Q. Y. *Mater. Sci. Eng., R* **2010**, *71*, 1–34.
- (16) Smet, P. F.; Parmentier, A. B.; Poelman, D. J. *J. Electrochem. Soc.* **2011**, *158*, R37–R54.
- (17) Xie, R.-J.; Hirosaki, N. *Sci. Technol. Adv. Mater.* **2007**, *8*, 588–600.
- (18) Zeuner, M.; Pagano, S.; Schnick, W. *Angew. Chem. Int. Ed. Engl.* **2011**, *50*, 7754–7775.
- (19) Xie, R.-J.; Hirosaki, N.; Sakuma, K.; Yamamoto, Y.; Mitomo, M. *Appl. Phys. Lett.* **2004**, *84*, 5404–5406.
- (20) Hirosaki, N.; Xie, R.-J.; Kimoto, K.; Sekiguchi, T.; Yamamoto, Y.; Suehiro, T.; Mitomo, M. *Appl. Phys. Lett.* **2005**, *86*, 211905.
- (21) Ueda, K.; Hirosaki, N.; Yamamoto, Y.; Naoto, A.; Nakajima, T.; Yamamoto, H. *Electrochim. Solid State Lett.* **2006**, *9*, H22–H25.
- (22) Li, Y. Q.; van Steen, J. E. J.; van Krevel, J. W. H.; Botty, G.; Delsing, A. C. A.; DiSalvo, F. J.; de With, G.; Hintzen, H. T. *J. Alloys Compd.* **2006**, *417*, 273–279.
- (23) Suehiro, T.; Hirosaki, N.; Xie, R.-J.; Sato, T. *Appl. Phys. Lett.* **2009**, *95*, 051903.
- (24) Hirosaki, N.; Xie, R.-J.; Inoue, K.; Sekiguchi, T.; Dierre, B.; Tamura, K. *Appl. Phys. Lett.* **2007**, *91*, 061101.
- (25) Ten Kate, O. M.; Hintzen, H. T.; Dorenbos, P.; van der Kolk, E. *J. Mater. Chem.* **2011**, *21*, 18289–18294.
- (26) Hoppe, H. A.; Lutz, H.; Morys, P.; Schnick, W.; Seilmeier, A. *J. Phys. Chem. Solids* **2000**, *61*, 2001–2006.
- (27) Hecht, C.; Stadler, F.; Schmidt, P.; Schnick, W. *Zeitschrift für anorganische und allgemeine Chemie* **2008**, *634*, 2044.
- (28) Oeckler, O.; Kechele, J. A.; Koss, H.; Schmidt, P. J.; Schnick, W. *Chem.—Eur. J.* **2009**, *15*, 5311–5319.
- (29) Hintze, F.; Hummel, F.; Schmidt, P. J.; Wiechert, D.; Schnick, W. *Chem. Mater.* **2012**, *24*, 402–407.
- (30) Kechele, J. A.; Hecht, C.; Oeckler, O.; auf der Günne, J. S.; Schmidt, P. J.; Schnick, W. *Chem. Mater.* **2009**, *21*, 1288–1295.
- (31) Danielson, E.; Golden, J. H.; McFarland, E. W.; Reaves, C. M.; Weinberg, W. H.; Wu, X. D. *Nature* **1997**, *389*, 944–948.
- (32) Sun, X. D.; Wang, K. A.; Yoo, Y.; Wallace-Freedman, W. G.; Gao, C.; Xiang, X.-D.; Schultz, P. G. *Adv. Mater.* **1997**, *9*, 1046–1049.
- (33) Danielson, E.; Devenney, M.; Giaquinta, D. M.; Golden, J. H.; Haushalter, R. C.; McFarland, E. W.; Poojary, D. M.; Reaves, C. M.; Weinberg, W. H.; Wu, X. D. *Science* **1998**, *279*, 837–839.
- (34) Wang, J.; Yoo, Y.; Gao, C.; Takeuchi, I.; Sun, X. D.; Chang, H.; Xiang, X.-D. *Science* **1998**, *279*, 1712–1714.
- (35) Park, W. B.; Singh, S. P.; Yoon, C.; Sohn, K. S. *J. Mater. Chem.* **2012**, *22*, 14068–14075.
- (36) Son, K. H.; Singh, S. P.; Sohn, K. S. *J. Mater. Chem.* **2012**, *22*, 8505–8511.
- (37) Park, W. B.; Shin, N.; Hong, K. P.; Pro, M.; Sohn, K. S. *Adv. Funct. Mater.* **2012**, *22*, 2258–2266.
- (38) Park, W. B.; Singh, S. P.; Sohn, K. S. *J. Am. Chem. Soc.* **2014**, *136*, 2363–2373.
- (39) Sheldrick, G. M. *SADABS, v.2: Multi-Scan Absorption Correction*; Bruker-AXS: Kennewick, WA, 2012.
- (40) Zhao, J.-C. *Prog. Mater. Sci.* **2006**, *51*, 557–631.
- (41) Maier, W. F.; Stowe, K.; Sieg, S. *Angew. Chem., Int. Ed.* **2007**, *46*, 6016–6067.
- (42) Sheldrick, G. M. *SHELXS97, Program for Crystal Structure Refinement*; University of Gottingen: Germany, 1997.
- (43) Sheldrick, G. M. *SHELXL97, Program for Crystal Structure Refinement*; University of Gottingen: Germany, 1997.
- (44) Ohkubo, K.; Shigeta, T. *J. Illum. Eng. Inst. Jpn.* **1999**, *83*, 87.
- (45) Li, H. L.; Xie, R.-J.; Zhou, G. H.; Hirosaki, N.; Sun, Z. J. *Electrochim. Soc.* **2010**, *157*, J251–J255.
- (46) Shioi, K.; Hirosaki, N.; Xie, R.-J.; Takeda, T.; Li, Y. Q. *J. Mater. Sci.* **2008**, *43*, 5659–5661.
- (47) Schlieper, T.; Milius, W.; Schnick, W. Z. *Anorg. Allg. Chem.* **1995**, *621*, 1380–1384.

- (48) Huppertz, H.; Schnick, W. *Chem.—Eur. J.* **1997**, *3*, 249–252.
- (49) Banchmann, V.; Ronda, C.; Meijerink, A. *Chem. Mater.* **2009**, *21*, 2077–2084.
- (50) Ruan, J.; Xie, R.-J.; Hirosaki, N.; Takeda, T. *J. Am. Ceram. Soc.* **2011**, *94*, 536–542.
- (51) Xie, R.-J.; Hirosaki, N.; Takeda, T.; Suehiro, T. *ECS J. Solid State Sci. Technol.* **2013**, *2*, R3031–R3034.
- (52) Huxtable, S.; Cahill, D. G.; Fauconnier, V.; White, J. O.; Zhao, J. *C. Nat. Mater.* **2004**, *3*, 298–301.
- (53) Potyrailo, K.; Rajan, K.; Stoewe, K.; Takeuchi, I.; Chisholm, B.; Lam, H. *ACS Comb. Sci.* **2011**, *13*, 579–633.